ACS OMEGA

http://pubs.acs.org/journal/acsodf

Article

Recovering and Exploiting Aragonite and Calcite Single Crystals with Biologically Controlled Shapes from Mussel Shells

Carla Triunfo, Stefanie Gärtner, Chiara Marchini, Simona Fermani, Gabriele Maoloni, Stefano Goffredo, Jaime Gomez Morales, Helmut Cölfen, and Giuseppe Falini*

Cite This: *ACS Omega* 2022, 7, 43992−43999

Read Online

ACCESS | Metrics & More | Article Recommendations | Supporting Information

ABSTRACT: Control over the shape and morphology of single crystals is a theme of great interest in fundamental science and for technological application. Many synthetic strategies to achieve this goal are inspired by biomineralization processes. Indeed, organisms are able to produce crystals with high fidelity in shape and morphology utilizing macromolecules that act as modifiers. An alternative strategy can be the recovery of crystals from biomineralization products, in this case, seashells. In particular, waste mussel shells from aquaculture are considered. They are mainly built up of single crystals of calcite fibers and aragonite tablets forming an outer and an inner layer, respectively. A simple mechanochemical treatment has been developed to separate and recover these two typologies of single crystals. The characterization of these single crystals showed peculiar properties with respect to the calcium carbonate from quarry or synthesis. We exploited these biomaterials in the water remediation field using them as substrate adsorbing dyes. We found that these substrates show a high capability of adsorption for anionic dye, such as Eosin Y, but a low capability of adsorption for cationic dyes, such as Blue Methylene. The adsorption was reversible at pH 5.6. This application represents just an example of the potential use of these biogenic single crystals. We also envision potential applications as reinforcing fillers and optical devices.

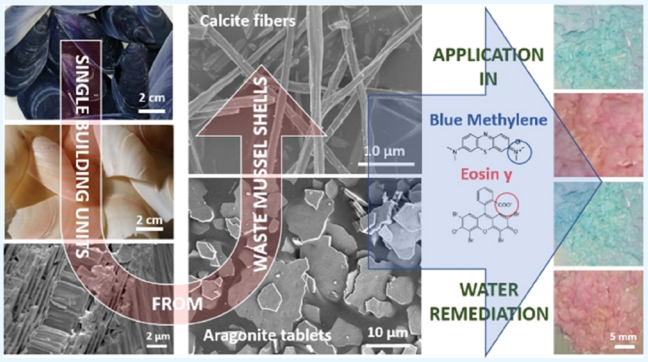

INTRODUCTION

Biominerals are biomineralization products that are commonly characterized by shape, morphology, polymorphism, and composition that differentiate them from their geogenic and synthetic counterparts.[1−3] The shell of the genus *Mytilus* is an example of biominerals characterized by three crystalline calcium carbonate regions: (i) the prismatic fibrous calcite, (ii) the aragonitic myostracum, and (iii) the aragonitic nacre. Each region has a species-specific crystal shape, morphology, and composition.[4−7]

In *Mytilus galloprovincialis,* the outer layer of the shell, referred to as the calcitic prismatic layer, is made of long, slender fibers of calcite (some 1−2 μm wide and hundreds of μm long), which reach the internal surface of the shell.[4] This microstructure has been called anvil-type fibrous calcite.[8] The myostracum is usually a very thin layer located in the attachment of the adductor muscle to the umbo of each valve. It is located under the calcitic prismatic layer and is in contact with the inner layer formed by the nacre.[9,7] It is made of aragonite.[10] The nacre is a well-defined type of microstructure characterized by small flat tablets (200−500 nm thick) of aragonite tightly packed together by a mineral bridge and an organic cement.[11−14] These peculiarities endow to the *M. galloprovincialis* shell with unique mechanical properties that have been optimized by millions of years of evolution upon the organism's survival needs.[15] These features have attracted the attention of researchers stimulating them to produce biomimetic and biologically inspired synthetic processes to obtain biomaterials similar to the biogenic ones in shape, morphology, and composition for different technological applications.[2] Although this approach has produced an impressive number of biomimetic minerals, materials that perform as the biogenic ones have been rarely obtained.

Thus, a more pragmatic approach has been the use of mollusk shells themselves. In this context, it has to be considered that mollusk shells are waste byproducts from mollusk aquaculture[16] that has a global production of mollusks of about 15 t per year (year 2015) in which *M. galloprovincialis* and *Mytilus edulis* count for about 1.5 t worldwide (year 2015).[17] Waste mussel shells have been used for different

Received: August 22, 2022
Accepted: October 31, 2022
Published: November 17, 2022

applications. They can be converted to calcium oxide by calcination and successfully used as catalysts for biodiesel production.[18] Seashells could be an inert material in concrete and other related cement-based products but heating at high temperature and crushing are required for high quality materials.[19] However, a life cycle assessment analysis revealed that the valuation of shell waste through a calcination process may not generate environmentally friendly after effects, as the impacts associated with the processing and treatment of shell waste might be greater than those associated with conventional end-of-life disposal methods.[19]

Taking into account these considerations, an innovative approach can be the waste mollusk shell valorization exploiting some of the unique features of biominerals, which are effectively biomaterials due to their physiochemical features and organic−inorganic composite structures.[1,20] Magnabosco et al. took advantage of the unique presence of the intraskeletal organic matrix to obtain covalent bond functionalization.[21] The intraskeletal organic matrix was also exploited to favor the polymeric coating of oyster shell particles to improve their metal ion adsorption.[22] The calcite fibers from the prismatic layer of the *Mytilus edulis* shell were used to obtain spherical aggregates of calcite fibers, exploiting their peculiar aspect ratio.[23]

Here we suggest the recovery and valorization of biomineral building units, namely, the fibrous calcite and the aragonite tablets by a simple and environmentally friendly procedure. This offers the possibility to overcome the synthetic difficulties in replicating the ability of organisms to act as crystal shapers and morphology modifiers and opens the possibility to use those crystals in purposes different from those for which they were biosynthetized. As a case of study, we used the fibrous calcite and the aragonite tablets as dye adsorbents in an envisioned water remediation application.

RESULTS

Mussel shells from a local market having an average length of 55 ± 35 mm were used after preliminary washing with tap water and brushing to remove meat residues and mineral debris. Then they were treated overnight with a 55% v/v NaClO solution. This provoked the oxidation and removal of the periostracum as well as superficial organic contaminants from the shells. The shells changed their color becoming more whitish (Figure S1). The content of the intraskeletal organic matrix, obtained by thermogravimetrical analysis, in the bleached shells was 1.1 ± 0.3 wt % (Table 1). After this stage, the shells were treated at a temperature of 220 °C for 48 h. This process provoked a mechanical separation of the external prismatic layer and the internal nacreous one (Figure 1A,B), while the myostracum layer remained attached to the external prismatic layer,[24,25] as can be observed in the scanning electron microscopy (SEM) images (see arrow in Figure 1C). The nacreous layer preserves its typical texture of casted tablets (Figure 1D).

The X-ray diffraction patterns showed only the presence of aragonite in the nacreous layer and the presence of calcite with trace (about 2.7 wt %) of aragonite in the prismatic layer, according to SEM observations (Figure 2 and Table 1). These results were also confirmed by the spectroscopic analysis (Figure S2).

The thermogravimetric analyses (TGA) of the two layers showed a content of intraskeletal organic material (structural water and organic matrix) of about 1.0 ± 0.1 wt % and 1.42 ± 0.02 wt % in the myostracum/prismatic layer and the nacre layer (Figure S3 and Table 1), respectively. Following this separation, the two main layers were subject to diverse treatments. The myostracum/prismatic layer was treated with a 5% v/v acetic acid solution for 24 h with the consequent complete dissolution of the myostracum, as shown by the absence of the diffraction peaks of aragonite in the diffraction pattern of the remaining prismatic calcite (Figure 2).

As the last preparative step, the treated prismatic calcite layer was lightly crushed, sieved at 600 μm, and bleached to remove the remaining superficial organic matrix. The obtained material was mainly constituted by single fibrous crystals of pure calcite (Figure S4A,B) containing an intraskeletal organic matrix of 0.041 ± 0.001 wt %, a surface area of 1.7 m^2/g, a particle size of 9.402 ± 0.037 μm, and an aspect ratio no lower than 5 (Figure 3A,B and Table S1). The thermally treated nacreous layers separated into almost single tablets after the removal of the intertablet organic matrix through a bleaching and sonication process (Figure S4C,D). After such a process, the organic matrix content remains unaltered (1.59 ± 0.02 wt %), indicating that the intercrystalline organic matrix was already eliminated by the thermal process (Figure S2) and the mineral phase remained as pure aragonite (Table 1). The surface area of this sample was 1.5 m^2/g. The single-crystal aragonite tablets were in majority single tablets, but particles formed by

Table 1. Percentage of Mineral Phase Composition Obtained by X-ray Diffraction, Intraskeletal Material (Structured Water and Organic Matrix) Content Obtained by Thermogravimetric Analyses and Particle Size of Bleached Mussel Shell (A), Nacre (B), Prismatic Layer and Myostracum (C), and Isolated Prismatic Layer (D)

sample	calcite (%)	aragonite (%)	intraskeletal material[a] (%)	D_{90}[b] (μm)
A	27.7 ± 0.3	72.3 ± 0.3	1.1 ± 0.3	
B		100	1.42 ± 0.02	13.76 ± 0.05
C	97.3 ± 0.4	2.7 ± 0.4	1.0 ± 0.1	
D	100		0.041 ± 0.001	9.402 ± 0.037

[a]The temperature range considered to estimate the content of intraskeletal organic material was between 150 and 450 °C. [b]D_{90} indicates that 90% of particles have a diameter below the reported value.

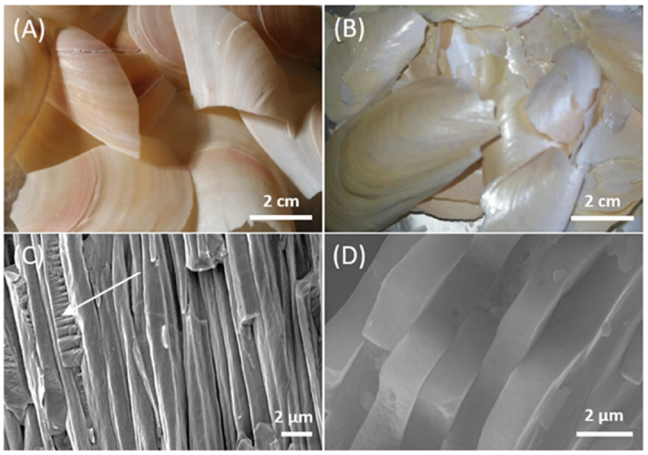

Figure 1. Camera and SEM images of the outer prismatic layer and myostracum (A,C) and the inner nacreous layer (B,D) after the thermal treatment. The myostracum layer is indicated by a white arrow.

https://doi.org/10.1021/acsomega.2c05386
ACS Omega 2022, 7, 43992−43999

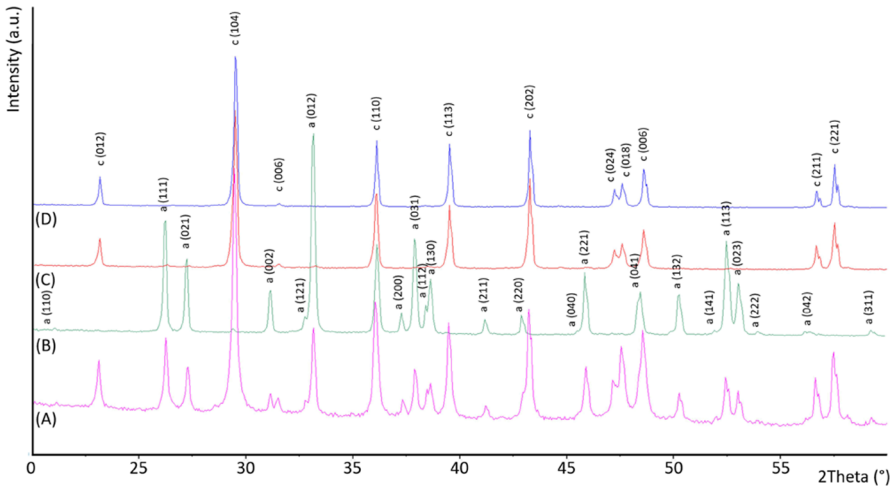

Figure 2. Powder X-ray diffraction patterns of mussel shell (A), nacre (B), and prismatic layer after the thermal (C) and acid treatment (D). The diffraction patterns were indexed accordingly to the PDF 00-005-0586 for calcite and PDF 00-005-0453 for aragonite.

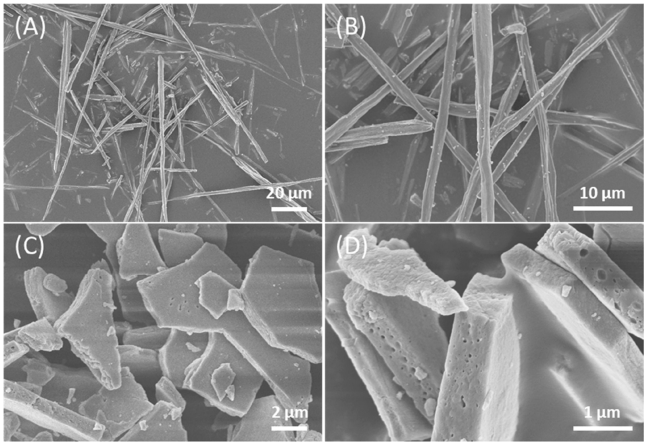

Figure 3. SEM images of isolated calcite fibers (A,B) and nacre tablets (C,D).

two or three casted tablets were also observed (Figure 3C,D). The SEM high-magnification images showed that on the surface of both kinds of crystals a nanoporosity was present, with pores having the longest axis in the range 20−180 nm (Figure S5).

The two typologies of single crystals, calcite and aragonite, were also tested for their capability to adsorb model dye molecules, Eosin Y (EY) and Blue Methylene (BM), in the perspective of their use as substrates for water remediation. The results of the isothermal adsorption experiments (Figure 4) showed that EY and BM have different adsorption profiles on the fibrous calcite and the tablets of aragonite.

The adsorption of the EY and BM on biogenic single crystals reaches equilibrium within 24 h (Figure 4A,B). In order to evaluate the adsorption kinetics mechanisms, the experimental data were fitted by pseudo-first-order and pseudo-second-order kinetic models.[26] The diffusion-based Weber−Morris model was tested as well.[27] It is noted that the pseudo-second-order kinetic model fits the adsorption data better than the pseudo-first-order model as indicated by higher R^2 values (Table 2).

EY isotherm absorption data fitted the best with a Langmuir isotherm with a Langmuir constant K_L = 0.12 and 0.19 L/mg, and q_{max} = 0.52 and 0.45 mg/g on fibrous calcite and aragonitic tablets, respectively (Table 3). The BM isothermal data fitted better with a Freundlich isotherm with K_F = 5.84 and 2.70 mg/g and n = 0.03 and 0.02 for adsorption on fibrous calcite and aragonitic nacre, respectively (Table 3). When considering the fitting using the Langmuir adsorption isotherm, the q_{max} of EY was higher than that of BM almost of a factor 10.

The desorption/dissolution experiment showed that at pH 6.0 or 7.2, the dyes were not removed from the substrates. At pH 5.6, a minimal dissolution (less than 5 wt %) of $CaCO_3$ was observed and the dyes were completely removed at a time interval of about 5 min. After this dye desorption/$CaCO_3$ dissolution process, single-crystal substrates were completely regenerated.

The ζ-potential of the crystals was measured in water, in the dye loading buffers, and after the dye adsorption. It was not possible to obtain a ζ-potential value for nacre tablets since the measurements were not homogeneous. For the calcite fibers, instead, the ζ-potential was −20.3 ± 0.6 mV in water (pH = 8.3), −11.6 ± 0.4 mV in the dye loading buffer (pH = 7.2) and − 15.4 ± 0.1 mV and − 19.8 ± 1.0 mV after the adsorption of EY and BM, respectively.

DISCUSSION

The sustainable and green production of biomaterials is a research theme of growing interest. Shells are waste byproducts from mollusk aquaculture and represent a sustainable type of food production since the mollusks, as herbivores, are low in the trophic chain. Mollusk shells are a biogenic source of calcium carbonate, and their potential as biomaterials has been poorly exploited so far. Their use as materials with a high added value can represent a perfect example of circular economy. If the market demand increases, this will be a trigger to increase production. The current study shows that by a simple thermal and chemical treatment it is possible to obtain surface organic matrix free single crystals of calcite and aragonite having the peculiar shape of long slender fibers and tablets, respectively. Synthetic calcite fibers with diameters ranging from 100 to 800 nm were produced by a polymer-induced liquid precursors (PILP) on existing calcite substrate crystals by the addition of poly(aspartic acid) to a crystallizing solution.[28] Nanofibers of calcite analogous to those produced via a PILP were produced using a positively charged additive poly(allylamine hydrochloride).[29] Nanowires of calcite particles precipitated in the pores, from 50 to 200 nm, of track

https://doi.org/10.1021/acsomega.2c05386
ACS Omega 2022, 7, 43992−43999

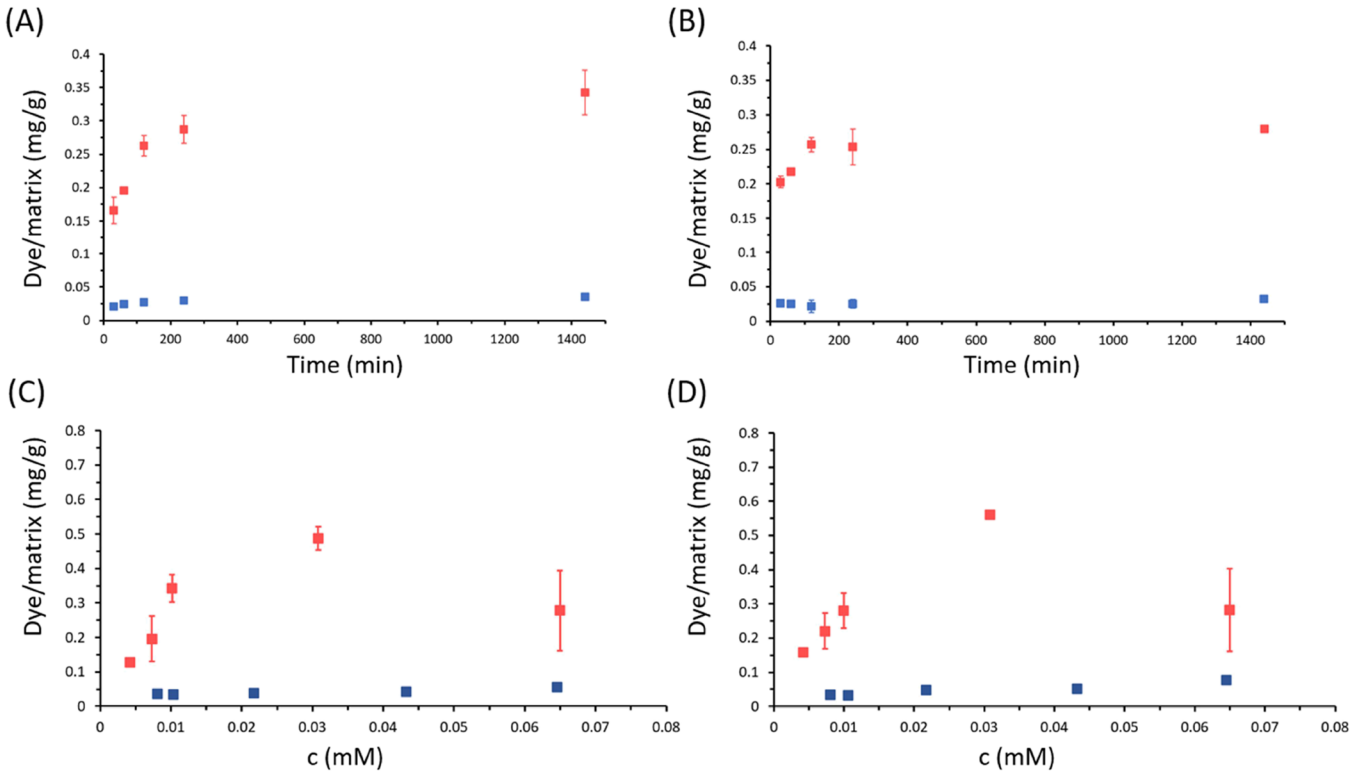

Figure 4. (A,B) Adsorption kinetics of BM (blue dots) and EY (red dots) 0.01 mM solutions at pH 7.2 on calcite fibers (A) and nacre tablets (B). (C,D) Adsorption isotherms of BM (blue dots) and EY (red dots) on calcite fibers (C) and nacre tablets (D). We suppose in both cases that adsorption equilibrium was achieved after an incubation time of 24 h. Dye adsorbed is reported as the mass of dye (mg), normalized over the mass of calcite fibers/nacre tablets (g). Error bars associated with BM measures are small and not visible in graphs.

Table 2. Parameters for Pseudo-First-Order and Pseudo-Second-Order As Well As Weber–Morris Models[a]

		pseudo-first-order model[b]			pseudo-second-order model[c]			Weber–Morris model[d]		
dye/substrate	$q_{max,\,exp}$ (mg g^{-1})	$q_{max,cal}$ (mg g^{-1})	k_1 (min^{-1})	R^2	$q_{max,cal}$ (mg g^{-1})	k_2 (g mg^{-1} min^{-1})	R^2	C (mg g^{-1})	k_{ip} (mg g^{-1} min$^{-1/2}$)	R^2
EY/calc. fib.	0.3424	0.2467	0.007	0.88	0.3265	0.089	0.95	0.1138	0.0074	0.66
EY/arag. tab.	0.2801	0.3433	0.002	0.49	0.2726	0.3128	0.91	0.1363	0.0051	0.43
BM/calc. fib.	0.0552	0.0269	0.083	0.72	0.05331	1.6211	0.96	0.026	0.001	0.44
BM/arag. tab.	0.0764	0.0532	0.0086	0.92	0.07584	0.5815	0.93	0.024	0.001	0.26

[a]The reaction conditions were based on 0.01 mM EY, 0.07 mM BM, and pH 7.2. [b]The pseudo-first-order model is given by $\ln (q_{max} - q_t) = \ln q_{max} - k_1 t$, where q_{max} and q_t are the amounts of adsorbed dye (EY or BM) at equilibrium and at time t (mg g^{-1}), respectively. k_1 is the equilibrium rate constant of pseudo-first-order kinetics (min^{-1}). [c]The pseudo-second-order model is determined by $1/q_t = 1/k_2 q_{max}^2\ 1/t + 1/q_{max}$, where k_2 is the equilibrium rate constant of the pseudo-second-order kinetics (g mg^{-1} min^{-1}). [d]The Weber–Morris model is expressed by $q_t = k_{ip} t^{1/2} + C$, where k_{ip} is the intraparticle diffusion rate constant (mg g^{-1} min$^{-1/2}$) and C (mg g^{-1}) is a constant that reflects the thickness of the boundary layer.

Table 3. Calculated Parameters from the Fitting of the Adsorption Isotherms with Different Models[a]

	Langmuir			Freundlich			Dubinin–Radushkevich		
dye/substrate	K_L (mg^{-1})	q_m (mg g^{-1})	R^2	K_F (mg g^{-1})	n	R^2	K_D (mol^2 kJ^{-2})	q_D (mg g^{-1})	R^2
EY/calc. fib.	0.12	0.52	**0.81**	0.13	3.20	0.45	2.1	0.37	0.77
EY/arag. tab.	0.19	0.45	**0.80**	0.14	3.52	0.46	0.99	0.17	0.65
BM/calc. fib.	0.85	0.05	0.71	5.84	0.03	**0.84**	0.99	0.16	0.55
BM/arag. tab.	0.310	0.07	0.84	2.70	0.02	**0.90**	1.02	0.06	0.68

[a]The R^2 values from the isotherm model(s) that indicated the best fitting are highlighted in bold.

etch membranes in the presence of acid macromolecules from a PILP precursor phase.[30] Into the same matrix, rod-like $CaCO_3$ crystals having a diameter of about 200 nm formed from amorphous calcium carbonate nanoparticles.[31−34] Via an amorphous precursor route, thin tablets (~600 nm thick) of aragonite were grown at the air–water interface using poly(acrylic acid–sodium salt) in combination with Mg^{2+} ion.[35] Mixed surfactant solutions of Ca and Mg dodecyl sulfate were used for the fabrication of pseudohexagonal and porous aragonite tablets with a triplet twinning and single-crystal-like nature.[36] Synthetic nacre, morphologically indistinguishable from the natural archetype, was synthesized with amorphous calcium carbonate precursors by confinement in the scaffold of the original insoluble nacre matrix.[37]

https://doi.org/10.1021/acsomega.2c05386
ACS Omega 2022, 7, 43992−43999

All these synthetic methods offered the advantage to have a rigorous control over shape, morphology, and composition, opening the possibility to produce single crystals with shapes and morphologies not observed in nature. On the other side, the production of massive amounts and the specificity on shape, morphology, composition, and polymorphism can be potential issues. Mussel shells, and in general many biominerals, are produced under biological control with high fidelity in crystal size, morphology, composition, and polymorphism. Moreover, the fine features of the crystalline units forming the shell can be modified by the environmental conditions in which the organism lives.[38]

Our research showed that by a simple chemical, thermal, and mechanical treatment the single-crystal building units—the fibrous calcite and the aragonite tablets—that form the mussel shell can be separated. These materials can have potential application in many fields, in optics,[39] polymer science,[40] medicine[41] and the paper industry,[42,43] among many others. $CaCO_3$ whiskers in paper were for example found to increase its strength.

Here we tested the use of single crystals of fibrous calcite and the aragonite tablets for water remediation. A powder from bivalve shells of *Anadara uropigimelana* was tested as a potential biosorbent for BM and showed a capability of adsorbing of 0.357 mg/g when a 0.06 mM (20 mg/L) BM loading solution was used. The surface area of this powder, which was calculated from the Langmuir adsorption isotherm, was 2.82 m^2/g.[44] Fibrous calcite from the mussel shell of *Mytilus edulis* was used for the removal of crystal violet from water solutions. It has a surface area of 37 m^2/g and showed a high loading capability (10 mg/g) from a 0.25 mM (100 mg/L) crystal violet solution.[23]

Our results showed that the two substrates were able to efficiently and in a reversible way to adsorb EY, bearing a negative charge, but were less efficient with BM (bearing a positive charge). The adsorption rate is an index for analyzing the adsorption process. The pseudo-first-order and the pseudo-second-order kinetic models were employed to fit the adsorption kinetics of EY and BM on the biogenic crystals.[45] The R^2 of the pseudo-second-order model was higher than that of the pseudo-first-order model in all cases (Table 2). This indicated that chemical adsorption is dominant.[46] Nevertheless, in the case of BM adsorption on aragonite tablets, a pseudo-first-order kinetic model is also suitable, because of the $R^2 > 0.90$ This suggests that there may be a physical adsorption during the adsorption process.[47] However, the maximum adsorption capacity (q_m) calculated by the pseudo-second-order model was much closer to the experimental maximum adsorption capacity than the pseudo-first-order (Table 2) in all cases, which further proved that the adsorption process of EY and BM on biogenic crystals conformed to the pseudo-second-order model. The steps involved in this kinetic model are: (i) molecules diffuse from the liquid phase to liquid−solid interface; (ii) molecules move from the liquid−solid interface to solid surfaces; and (iii) molecules diffuse into the particle pores.[48] Herein, the first step is not rate-limited because the adsorption was performed under shaking conditions. The rate constant (k_2) of BM is higher than that of EY suggesting an initial faster occupation of the adsorption sites on the solid surface.

The study of the isotherm models indicates that the Langmuir isotherm is more suitable to describe the adsorption process of EY. This suggests a chemically controlled adsorption which is dominated by a monolayer formation, as also suggested by the kinetic analysis.[49] The driving force for the adsorption should be, in accordance with the value of K_L, the formation of a strong coordination chemical bond involving calcium ions between the mineral surface and EY. Here, according to the Langmiur model, we reach 0.52 mg/g adsorption capacity for EY on the calcite fibers and 0.45 mg/g for the aragonite tablets, which are higher than literature results of 0.357 mg/g reported for BM, also considering the lower surface area (about 1.5 m^2/g vs 2.8 m^2/g).[44]

The adsorption of BM is better described by a Freundlich isotherm, indicating a no site-specific interaction and formation of multilayers. The fibrous calcite surface has a negative charge that is pH dependant and we can suppose the same for the aragonite tablets. In the loading buffer (pH = 7.2) upon adsorption of dyes, EY or BM, there is an increase of the ζ-potential, more marked for BM (from −11.6 to −15.4 mV for EY and − 19.8 mV for BM). To understand these unexpected results, EY and BM having different charge, it can be supposed that other reactions can occur on the thermally treated and oxidized biogenic crystal surfaces, beside the expected electrostatic interaction. It has been reported that biogenic crystals have low crystalline order on their surface, even the presence of amorphous calcium carbonate,[50,51] and that after thermal treatment the carbonate groups are replaced by hydroxyl groups.[52] The combination of these two effects can change the mechanisms of interaction of dyes. The isotherm data indicate that BM, positively charged, adsorbs on the biogenic calcite surface sites mainly by direct and fast no site-specific electrostatic interactions. Differently, the adsorption of EY, negatively charged on its carboxylate groups, should occur through the formation of a cationic coordination bond with the calcium ions present in solution; in this process, the surface hydroxyl groups can participate in the coordination bonding of calcium ions without affecting the net charge.

It is also of interest the comparison over the experimental adsorption capability of the two polymorph substrates. The single crystals of fibrous calcite and tablet aragonite show a similar EY adsorption capability for surface unit, 0.20 and 0.19 mg/m^2, respectively. This may seem unexpected since calcite and aragonite have different crystal structures and expose different crystalline faces.[53] However, the proposed surface structural re-organization, which produces surface hydroxyl groups,[52] can be considered to justify this similarity. The adsorption of BM, which occurs via no site-specific interactions (i.e., Freundlich isotherm), was slightly higher on aragonite tablets (0.052 mg/m^2) than on fibrous calcite (0.032 mg/m^2). This difference could be nonsignificant, considering the low loading capability. In general, the loading capability of the proposed biogenic single-crystal substrates is lower than that of other nonmineral materials,[54] and the here described materials offer the advantage to be re-used since the dye desorption/dissolution occurs under slightly acid conditions.

CONCLUSIONS

This research showed that single crystals of calcite and aragonite with a biologically controlled shape and morphology can be obtained from mussel shells by chemical and mechanical treatments. The separation process implies simple and sustainable processes. The obtained single crystals, due to their unique and no lab reproducible aspect ratio, can have many potential applications. Here, they were used as a substrate for reversible dye removal, but other potential

https://doi.org/10.1021/acsomega.2c05386
ACS Omega 2022, 7, 43992−43999

applications are foreseen as filler to improve the mechanical properties of matrices or as part of optical devices.

MATERIALS AND METHODS

Reagents and solvents were purchased from Merk. They were utilized without any further purification. For each experiment, daily fresh solutions were prepared. Mussels of *M. galloprovincialis* from Spain aquaculture were purchased. The shells were first washed with tap water to eliminate the meat residues and mineral debris and then mechanically stirred in a 5% v/v sodium hypochlorite solution for 24 h (1 g of shells in 10 mL solution). The shells were separated from the solution by decanting, washed with water, and air-dried. Next, they were heated in an oven at 220 °C for 48 h and the thermal treatment allowed the mechanical separation of the inner nacreous layer from the outer prismatic layer of the shell.

Prismatic Layer Treatment for Calcite Fiber Disassembly. The prismatic layer fragments were mechanically stirred in a 5% v/v acetic acid solution for 24 h in order to remove the remaining aragonitic layer of myostracum (2.2 g of fragments in 25 mL solution). The fragments were separated from the solution by decanting, washed with water, and air-dried. The isolated calcite layer fragments were then crushed by a mortar and pestle, sieved at 600 μm, and bleached.

Nacreous Layer Treatment for Tablet Disassembly. The nacreous layer fragments were crushed by a mortar and pestle and sieved at 45 μm. The nacreous powder was mechanically stirred in a 5% v/v sodium hypochlorite solution for 24 h (1 g of powder in 10 mL solution) and then bath sonicated in the same solution for 15 min. The resulting suspension was centrifuged at 5000 rpm for 2 min and the supernatant was discarded. The nacreous powder was then washed three times with water by a centrifuge (5000 rpm, 2 min) and the isolated powder was dried under vacuum in a desiccator overnight.

X-ray Powder Diffraction Analysis. X-ray diffraction patterns were collected using a PanAnalytical X'Pert Pro diffractometer equipped with a multiarray X'Celerator detector using Cu Kα radiation generated at 40 kV and 40 mA (λ = 1.54056 Å). The diffraction patterns were collected in the 2θ range between 20 and 60° with a step size ($\Delta 2\theta$) of 0.05° and a counting time of 60 s.

Spectroscopic Analysis. A Thermo Scientific Nicolet iS10 FTIR Spectrometer was used to collect the FTIR spectra. The disk sample for Fourier transform infrared (FTIR) analysis was obtained by mixing a small amount (2 mg) of product with 100 mg of KBr and applying a pressure of 45 tsi (620.5 MPa) to the mixture using a press. The spectra were obtained with 4 cm^{-1} resolution and 64 scans.

Thermal Analysis. TGA was performed using an SDT Q600 V 8.0 instrument (TA Instruments). The system was pre-equilibrated at 30 °C, then a ramp from 30 to 600 °C with a 10 °C min^{-1} heating rate was performed under nitrogen flow. The measurement was performed three times on 20 mg of each sample. The temperature range considered to estimate the content of the intraskeletal organic matrix was between 150 and 450 °C.

Brunauer–Emmett–Teller Analysis. The specific surface area of the samples was measured by the multiple Brunauer–Emmett–Teller (BET) method using a Gemini VII 2390 Series Surface Area Analyzer (Micromeritics Instrument Corporation) with a nitrogen flow. Prior to performing the BET analysis, samples (approx. 0.10–0.50 g) were thermostated at 150 °C under a nitrogen flow for 3 h and cooled down at room temperature under a nitrogen flow for further 30 min.

Dimensional Distribution Analysis. Particle size analyses were performed using a Mastersizer 3000 laser diffraction particle size analyzer. The particles from each sample were dispersed in isopropanol for the measurement.

SEM. All SEM images were acquired using a ZEISS Leo 1530 Gemini field emission scanning electron microscope operating at 5 kV. All samples were dried under vacuum in a desiccator and gold-coated before their observation.

ζ-Potential Analysis. The ζ-potential of the particles was evaluated using a Malvern Zetasizer Nano ZS equipped with a He-Ne laser source (633 nm, 5 mW).

Dye Adsorption Kinetics Experiments. Adsorption kinetics experiments were carried out suspending 50 mg of each material in 10 mL of dye in a 50 mM pH 7.2 bis-tris buffer solution. The suspensions were kept in 15 mL polypropylene conical centrifuge tubes at room temperature under mechanical stirring. Two dyes were tested, BM and EY, both having an absorption maximum in the visible region (668 and 517 nm, respectively). The dye concentration in solution was measured by a UV–Vis spectrophotometer (Cary 300 Bio, Agilent Technologies) using a spectral range of 450–800 nm and the spectra were recorded after 30 min, 1, 2, 4, and 24 h. For each measurement, the dye solution was centrifuged at 10,000 rpm for 90 s and the supernatant was transferred into a plastic cuvette with 1 cm optical path.

Dye Desorption Experiments. Desorption kinetics experiments were carried out suspending 25 mg of each sample from the dye adsorption experiments in 5 mL of a 50 mM pH 5.6 citrate buffer solution. The suspensions were kept in 15 mL polypropylene conical centrifuge tubes at room temperature under mechanical stirring and the concentration of the dye released in the solution was measured using the same procedure of the adsorption experiments.

ASSOCIATED CONTENT

Supporting Information

The Supporting Information is available free of charge at https://pubs.acs.org/doi/10.1021/acsomega.2c05386.

> Camera images of mussel shells before and after bleaching with NaClO 5% v/v solution; size distribution of the isolated prismatic layer and nacre; FTIR spectra of mussel shell, nacre, prismatic layer and myostracum, and isolated prismatic layer; TGA profiles of bleached mussel shell, nacre, prismatic layer, and myostracum and isolated prismatic layer; optical microscopy images of isolated calcite fibers and nacre tablets; high-magnification SEM images of a single crystal of fibrous calcite and tablet nacre; size distribution of the isolated prismatic layer and nacre (PDF)

AUTHOR INFORMATION

Corresponding Author

Giuseppe Falini − *Department of Chemistry "Giacomo Ciamician", University of Bologna, 40126 Bologna, Italy;* orcid.org/0000-0002-2367-3721; Email: giuseppe.falini@unibo.it

https://doi.org/10.1021/acsomega.2c05386
ACS Omega 2022, 7, 43992−43999

Authors

Carla Triunfo − *Department of Chemistry "Giacomo Ciamician", University of Bologna, 40126 Bologna, Italy; Fano Marine Center, The Inter-Institute Center for Research on Marine Biodiversity, Resources and Biotechnologies, 61032 Fano, Italy*

Stefanie Gärtner − *Department of Chemistry, Physical Chemistry, University of Konstanz, D-78457 Konstanz, Germany*

Chiara Marchini − *Department of Chemistry "Giacomo Ciamician", University of Bologna, 40126 Bologna, Italy; Fano Marine Center, The Inter-Institute Center for Research on Marine Biodiversity, Resources and Biotechnologies, 61032 Fano, Italy*

Simona Fermani − *Department of Chemistry "Giacomo Ciamician", University of Bologna, 40126 Bologna, Italy; Interdepartmental Centre for Industrial Research Health Sciences and Technologies, University of Bologna, 40064 Bologna, Italy*

Gabriele Maoloni − *Plant Ascoli Piceno, Finproject S.p.A., 3100 Ascoli Piceno, Italy*

Stefano Goffredo − *Fano Marine Center, The Inter-Institute Center for Research on Marine Biodiversity, Resources and Biotechnologies, 61032 Fano, Italy; Department of Biological, Geological and Environmental Sciences, University of Bologna, 40126 Bologna, Italy*

Jaime Gomez Morales − *Laboratorio de Estudios Cristalográficos, Instituto Andaluz de Ciencias de la Tierra (CSIC-UGR), 18100 Armilla (Granada), Spain;* orcid.org/0000-0002-9395-7797

Helmut Cölfen − *Department of Chemistry, Physical Chemistry, University of Konstanz, D-78457 Konstanz, Germany;* orcid.org/0000-0002-1148-0308

Complete contact information is available at: https://pubs.acs.org/10.1021/acsomega.2c05386

Author Contributions

The manuscript was written through contributions of all authors. All authors have given approval to the final version of the manuscript.

Funding

Bluebio ERANET project CASEAWA (grant no.: 161B0949).

Notes

The authors declare no competing financial interest.

■ ACKNOWLEDGMENTS

This research was performed under the Bluebio ERANET project CASEAWA (grant no.: 161B0949). This study represents partial fulfillment of the requirements for the International FishMed-PhD thesis of C.T. J.G.M acknowledges the CASEAWA project, grant no. PCI2020-112108 funded by MCIN/AEI/10.13039/501100011033 (Spain) and the EU "NextGenerationEU"/PRTR". PCI2020-112108 is part of the ERANET Cofund BlueBio Programme supported by the European Union.

■ REFERENCES

(1) Lowenstam, H. A.; Weiner, S. *On Biomineralization*; Oxford University Press on Demand, 1989.

(2) Meldrum, F. C.; Cölfen, H. Controlling Mineral Morphologies and Structures in Biological and Synthetic Systems. *Chem. Rev.* **2008**, *108*, 4332−4432.

(3) Meldrum, F. C. Calcium Carbonate in Biomineralisation and Biomimetic Chemistry. *Int. Mater. Rev.* **2003**, 187−224.

(4) Grégoire, C. Structure of the Conchiolin Cases of the Prisms in Mytilus Edulis Linne. *J. Cell Biol.* **1961**, *9*, 395−400.

(5) Grenier, C.; Román, R.; Duarte, C.; Navarro, J. M.; Rodriguez-Navarro, A. B.; Ramajo, L. The Combined Effects of Salinity and PH on Shell Biomineralization of the Edible Mussel Mytilus Chilensis. *Environ. Pollut.* **2020**, *263*, No. 114555.

(6) Gao, P.; Liao, Z.; Wang, X.; Bao, L.; Fan, M.; Li, X.; Wu, C.; Xia, S. Layer-by-Layer Proteomic Analysis of Mytilus Galloprovincialis Shell. *PLoS One* **2015**, *10*, No. e0133913.

(7) Kennedy, W. J.; Taylor, J. D.; Hall, A. Environmental and Biological Controls on Bivalve Shell Mineralogy. *Biol. Rev.* **1969**, *44*, 499−530.

(8) Checa, A. G.; Pina, C. M.; Osuna-Mascaró, A. J.; Rodríguez-Navarro, A. B.; Harper, E. M. Crystalline Organization of the Fibrous Prismatic Calcitic Layer of the Mediterranean Mussel Mytilus Galloprovincialis. *Eur. J. Mineral.* **2014**, *26*, 495−505.

(9) Oberling, J.-J. Observations on Some Structural Features of the Pelecypod Shell. *Mitt. Naturforsch. Ges. Bern* **1964**, *20*, 1−60.

(10) Castro-Claros, J. D.; Checa, A.; Lucena, C.; Pearson, J. R.; Salas, C. Shell-Adductor Muscle Attachment and Ca^{2+} Transport in the Bivalves Ostrea Stentina and Anomia Ephippium. *Acta Biomater.* **2021**, *120*, 249−262.

(11) Cartwright, J. H. E.; Checa, A. G. The Dynamics of Nacre Self-Assembly. *J. R. Soc., Interface* **2007**, *4*, 491−504.

(12) Addadi, L.; Weiner, S. A Pavement of Pearl. *Nature* **1997**, *389*, 912−913.

(13) Göppert, A.; Cölfen, H. Infiltration of Biomineral Templates for Nanostructured Polypyrrole. *RSC Adv.* **2018**, *8*, 33748−33752.

(14) Cartwright, J. H. E.; Checa, A. G.; Escribano, B.; Sainz-Díaz, C. I. Spiral and Target Patterns in Bivalve Nacre Manifest a Natural Excitable Medium from Layer Growth of a Biological Liquid Crystal. *Proc. Natl. Acad. Sci. U. S. A.* **2009**, *106*, 10499−10504.

(15) Knoll, A. H. Biomineralization and Evolutionary History. *Rev. Mineral. Geochem.* **2003**, *54*, 329−356.

(16) Morris, J. P.; Backeljau, T.; Chapelle, G. Shells from Aquaculture: A Valuable Biomaterial, Not a Nuisance Waste Product. *Rev. Aquac.* **2019**, *11*, 42−57.

(17) FAO; The State of World Fisheries and Aquaculture. *Sustainability in Action*; FAO: Rome, Italy, 2020.

(18) Rezaei, R.; Mohadesi, M.; Moradi, G. R. Optimization of Biodiesel Production Using Waste Mussel Shell Catalyst. *Fuel* **2013**, *109*, 534−541.

(19) Mo, K. H.; Alengaram, U. J.; Jumaat, M. Z.; Lee, S. C.; Goh, W. I.; Yuen, C. W. Recycling of Seashell Waste in Concrete: A Review. *Constr. Build. Mater.* **2018**, *162*, 751−764.

(20) Addadi, L.; Weiner, S. Biomineralization: Mineral Formation by Organisms. *Phys. Scr.* **2014**, *89*, No. 098003.

(21) Magnabosco, G.; Giuri, D.; Di, A. P.; Scarpino, F.; Fermani, S.; Tomasini, C.; Falini, G. New Material Perspective for Waste Seashells by Covalent Functionalization. *ACS Sustainable Chem. Eng.* **2021**, *9*, 6203−6208.

(22) Zhou, X.; Liu, W.; Tian, C.; Mo, S.; Liu, X.; Deng, H.; Lin, Z. Mussel-Inspired Functionalization of Biological Calcium Carbonate for Improving Eu(III) Adsorption and the Related Mechanisms. *Chem. Eng. J.* **2018**, *351*, 816−824.

(23) Murphy, J. N.; Schneider, C. M.; Hawboldt, K.; Kerton, F. M. Hard to Soft: Biogenic Absorbent Sponge-like Material from Waste Mussel Shells. *Matter* **2020**, *3*, 2029−2041.

(24) Bourgoin, B. P. A Rapid and Inexpensive Technique to Separate the Calcite and Nacreous Layers in Mytilus Edulis Shells. *Mar. Environ. Res.* **1988**, *25*, 125−129.

(25) Murphy, J. N.; Schneider, C. M.; Mailänder, L. K.; Lepillet, Q.; Hawboldt, K.; Kerton, F. M. Wealth from Waste: Blue Mussels (Mylitus Edulis) Offer up a Sustainable Source of Natural and Synthetic Nacre. *Green Chem.* **2019**, *21*, 3920−3929.

(26) Tanis, E.; Hanna, K.; Emmanuel, E. Experimental and Modeling Studies of Sorption of Tetracycline onto Iron Oxides-Coated Quartz. *Colloids Surf., A* **2008**, *327*, 57−63.
(27) Wang, X.; Shu, L.; Wang, Y.; Xu, B.; Bai, Y.; Tao, S.; Xing, B. Sorption of Peat Humic Acids to Multi-Walled Carbon Nanotubes. *Environ. Sci. Technol.* **2011**, *45*, 9276−9283.
(28) Olszta, M. J.; Gajjeraman, S.; Kaufman, M.; Gower, L. B. Nanofibrous Calcite Synthesized via a Solution−Precursor−Solid Mechanism. *Chem. Mater.* **2004**, *16*, 2355−2362.
(29) Cantaert, B.; Verch, A.; Kim, Y.-Y.; Ludwig, H.; Paunov, V. N.; Kröger, R.; Meldrum, F. C. Formation and Structure of Calcium Carbonate Thin Films and Nanofibers Precipitated in the Presence of Poly(Allylamine Hydrochloride) and Magnesium Ions. *Chem. Mater.* **2013**, *25*, 4994−5003.
(30) Kim, Y.; Hetherington, N. B. J.; Noel, E. H.; Kröger, R.; Charnock, J. M.; Christenson, H. K.; Meldrum, F. C. Capillarity Creates Single-crystal Calcite Nanowires from Amorphous Calcium Carbonate. *Angew. Chem., Int. Ed.* **2011**, *123*, 12780−12785.
(31) Xu, Y.; Tijssen, K. C. H.; Bomans, P. H. H.; Akiva, A.; Friedrich, H.; Kentgens, A. P. M.; Sommerdijk, N. A. J. M. Microscopic Structure of the Polymer-Induced Liquid Precursor for Calcium Carbonate. *Nat. Commun.* **2018**, *9*, 2582.
(32) Kajiyama, S.; Nishimura, T.; Sakamoto, T.; Kato, T. Aragonite Nanorods in Calcium Carbonate/Polymer Hybrids Formed through Self-Organization Processes from Amorphous Calcium Carbonate Solution. *Small* **2014**, *10*, 1634−1641.
(33) Nakayama, M.; Kajiyama, S.; Nishimura, T.; Kato, T. Liquid-Crystalline Calcium Carbonate: Biomimetic Synthesis and Alignment of Nanorod Calcite. *Chem. Sci.* **2015**, *6*, 6230−6234.
(34) Nakayama, M.; Kajiyama, S.; Kumamoto, A.; Ikuhara, Y.; Kato, T. Bioinspired Selective Synthesis of Liquid-Crystalline Nanocomposites: Formation of Calcium Carbonate-Based Composite Nanodisks and Nanorods. *Nanoscale Adv.* **2020**, *2*, 2326−2332.
(35) Amos, F. F.; Sharbaugh, D. M.; Talham, D. R.; Gower, L. B.; Fricke, M.; Volkmer, D. Formation of Single-Crystalline Aragonite Tablets/Films via an Amorphous Precursor. *Langmuir* **2007**, *23*, 1988−1994.
(36) Liu, F.; Gao, Y.; Zhao, S.; Shen, Q.; Su, Y.; Wang, D. Biomimetic Fabrication of Pseudohexagonal Aragonite Tablets through a Temperature-Varying Approach. *Chem. Commun.* **2010**, *46*, 4607−4609.
(37) Gehrke, N.; Nassif, N.; Pinna, N.; Antonietti, M.; Gupta, H. S.; Cölfen, H. Retrosynthesis of Nacre via Amorphous Precursor Particles. *Chem. Mater.* **2005**, *17*, 6514−6516.
(38) Gilbert, P. U. P. A.; Bergmann, K. D.; Myers, C. E.; Marcus, M. A.; DeVol, R. T.; Sun, C.-Y.; Blonsky, A. Z.; Tamre, E.; Zhao, J.; Karan, E. A.; Tamura, N.; Lemer, S.; Giuffre, A. J.; Giribet, G.; Eiler, J. M.; Knoll, A. H. Nacre Tablet Thickness Records Formation Temperature in Modern and Fossil Shells. *Earth Planet. Sci. Lett.* **2017**, *460*, 281−292.
(39) Sulimai, N. H.; Rani, R. A.; Khusaimi, Z.; Abdullah, S.; Salifairus, M. J.; Alrokayan, S.; Khan, H.; Sermon, P. A.; Rusop, M. Facile Synthesis of $CaCO_3$ and Investigation on Structural and Optical Properties of High Purity Crystalline Calcite. *Mater. Sci. Eng., B* **2019**, *243*, 78−85.
(40) Zuiderduin, W. C. J.; Westzaan, C.; Huétink, J.; Gaymans, R. J. Toughening of Polypropylene with Calcium Carbonate Particles. *Polymer* **2003**, *44*, 261−275.
(41) Magnabosco, G.; Giosia, M.; Polishchuk, I.; Weber, E.; Fermani, S.; Bottoni, A.; Zerbetto, F.; Pelicci, P. G.; Pokroy, B.; Rapino, S.; et al. Calcite Single Crystals as Hosts for Atomic-Scale Entrapment and Slow Release of Drugs. *Adv. Healthcare Mater.* **2015**, *4*, 1510−1516.
(42) Smith, C. A. Calcium Carbonate as a Pigment for Paper Coating: A Review of the Properties and Applications with Particular Reference to the Paper Industry. *Pigm. Resin Technol.* **1982**, *11*, 15−16.
(43) Chen, X.; Qian, X.; An, X. Using Calcium Carbonate Whiskers as Papermaking Filler. *BioResources* **2011**, *6*, 2435−2447.
(44) Elwakeel, K. Z.; Elgarahy, A. M.; Mohammad, S. H. Use of Beach Bivalve Shells Located at Port Said Coast (Egypt) as a Green Approach for Methylene Blue Removal. *J. Environ. Chem. Eng.* **2017**, *5*, 578−587.
(45) Liao, P.; Yuan, S.; Xie, W.; Zhang, W.; Tong, M.; Wang, K. Adsorption of Nitrogen-Heterocyclic Compounds on Bamboo Charcoal: Kinetics, Thermodynamics, and Microwave Regeneration. *J. Colloid Interface Sci.* **2013**, *390*, 189−195.
(46) Kubo, M.; Moriyama, R.; Shimada, M. Facile Fabrication of HKUST-1 Nanocomposites Incorporating Fe_3O_4 and TiO_2 Nanoparticles by a Spray-Assisted Synthetic Process and Their Dye Adsorption Performances. *Microporous Mesoporous Mater.* **2019**, *280*, 227−235.
(47) Li, Q.; Sun, J.; Ren, T.; Guo, L.; Yang, Z.; Yang, Q.; Chen, H. Adsorption Mechanism of 2,4-Dichlorophenoxyacetic Acid onto Nitric-Acid-Modified Activated Carbon Fiber. *Environ. Technol.* **2018**, *39*, 895−906.
(48) Ho, Y. S.; McKay, G. Pseudo-Second Order Model for Sorption Processes. *Process Biochem.* **1999**, *34*, 451−465.
(49) Wang, W.; Zhang, H.; Feng, S.; San Emeterio, J.; Mallapragada, S.; Vaknin, D. Iron Ion and Iron Hydroxide Adsorption to Charge-Neutral Phosphatidylcholine Templates. *Langmuir* **2016**, *32*, 7664−7670.
(50) Gong, Y. U. T.; Killian, C. E.; Olson, I. C.; Appathurai, N. P.; Amasino, A. L.; Martin, M. C.; Holt, L. J.; Wilt, F. H.; Gilbert, P. Phase Transitions in Biogenic Amorphous Calcium Carbonate. *Proc. Natl. Acad. Sci. U. S. A.* **2012**, *109*, 6088−6093.
(51) Baronnet, A.; Cuif, J.-P.; Dauphin, Y.; Farre, B.; Nouet, J. Crystallization of Biogenic Ca-Carbonate within Organo-Mineral Micro-Domains. Structure of the Calcite Prisms of the Pelecypod Pinctada Margaritifera (Mollusca) at the Submicron to Nanometre Ranges. *Mineral. Mag.* **2008**, *72*, 617−626.
(52) Ban, M.; Luxbacher, T.; Lützenkirchen, J.; Viani, A.; Bianchi, S.; Hradil, K.; Rohatsch, A.; Castelvetro, V. Evolution of Calcite Surfaces upon Thermal Decomposition, Characterized by Electrokinetics, in-Situ XRD, and SEM. *Colloids Surf., A* **2021**, *624*, No. 126761.
(53) Niu, Y.-Q.; Liu, J.-H.; Aymonier, C.; Fermani, S.; Kralj, D.; Falini, G.; Zhou, C.-H. Calcium Carbonate: Controlled Synthesis, Surface Functionalization, and Nanostructured Materials. *Chem. Soc. Rev.* **2022**, *51*, 7883−7943.
(54) Montroni, D.; Piccinetti, C.; Fermani, S.; Calvaresi, M.; Harrington, M. J.; Falini, G. Exploitation of Mussel Byssus Mariculture Waste as a Water Remediation Material. *RSC Adv.* **2017**, *7*, 36605−36611.

https://doi.org/10.1021/acsomega.2c05386
ACS Omega 2022, 7, 43992−43999